

# Nonlinear Time-Domain Analysis of Injection-Locked Microwave MESFET Oscillators

Jonathan Dixon, *Student Member, IEEE*, Elizabeth Bradley, *Member, IEEE*, and Zoya B. Popović, *Member, IEEE*

**Abstract**—In this paper, injection-locked MESFET oscillators are analyzed using several numerical models. The injection-locking behavior of the van der Pol equation and of a more complex representation using the Curtice–Cubic MESFET model are investigated. Analysis and experimental results are compared for an NE71083 transistor oscillator operating at 0.5 GHz. The deficiencies of using a van der Pol oscillator model are pointed out. Time-domain results from the complex model exhibiting multicycle and apparently chaotic behaviors are also examined, and point to problems with common nonlinear simulation techniques for these circuits.

**Index Terms**—Chaos, injection-locking, nonlinear modeling, transistor oscillator.

## I. INTRODUCTION

THE USE of linear models to predict oscillator behavior suffers from many limitations, which make it difficult to accurately predict operating frequency and power. As attempts are made to improve oscillator performance by setting operating points farther into nonlinear regimes, the ability to model these effects becomes critical, since saturation can influence frequency of operation, power output, and efficiency. Designing better oscillators requires a more complete understanding of how the nonlinear aspects of the oscillator affect its operation.

In addition, interest in nonlinear coupling behavior has increased due to the recent advances in free-space power combining [1]–[8] and phase-shifterless beam scanning [9], [10]. Because these types of combiners involve a large number of coupled oscillators, an understanding of the coupling mechanisms is critical to improving the phase noise, tuning, and locking ability.

As a starting point for understanding coupling behavior in microwave oscillators, the authors have chosen to examine the source–load oscillator topology, shown in Fig. 1. This topology is simple enough that the analysis does not depend upon too many components, but is still complex enough to show the different behaviors common in microwave oscillators.

In the past, the primary approaches to nonlinear oscillator modeling have been harmonic-balance simulations [11] and

Manuscript received July 25, 1996; revised March 24, 1997. This work was supported by the Office of Naval Research under a Graduate Fellowship, by the National Science Foundation under an NSF Presidential Faculty Fellowship, and an NSF National Young Investigator Award CCR-9 357 740.

J. Dixon and Z. B. Popović are with the Electrical Engineering and Computer Engineering Department, University of Colorado, Boulder, CO 80309 USA.

E. Bradley is with the Department of Computer Science, University of Colorado, Boulder, CO 80309 USA.

Publisher Item Identifier S 0018-9480(97)04454-2.

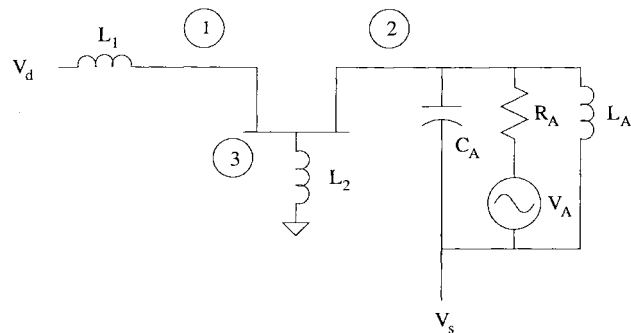


Fig. 1. Source–load oscillator topology with the circuit nodes numbered. Node 2 is the source of the transistor, which is coupled to a tank circuit and drive voltage.

the Volterra series method [12]. In both of these, the calculations are performed in the frequency domain, assuming constant or slowly varying amplitudes, and the results are then converted back into the time domain. The van der Pol equation [13] has also been used to model time-domain characteristics of coupled microwave oscillators, but there has been little work on time-domain modeling of injection-locked oscillators using more realistic models.

In this paper, results from two numerical models are compared—the van der Pol oscillator equation and a more realistic representation using a more complicated transistor model—with experimental results. While this particular analysis uses the Curtice–Cubic transistor model, it can be extended to a wide variety of other nonlinear transistor models. The implications of the authors’ time-domain analysis on traditional microwave oscillator modeling and design are also examined.

## II. NUMERICAL METHODOLOGY FOR ANALYSIS OF INJECTION-LOCKED OSCILLATOR MODELS

One common way of characterizing dynamic behavior of nonlinear systems is the parametric sweep, where several system parameters are varied and the behavior of the resulting system is examined [14] and typically presented as a parameter-space portrait. In this study of the injection-locking characteristics, the parameters varied are the magnitude and frequency of the injected signal. For this paper’s numerical experiments, this sweep in drive frequency and magnitude is implemented by stepping loops within the main program.

Automation of the sweep process requires a method that allows the computer to determine whether the oscillator is locked to the injected signal. One way of judging whether a

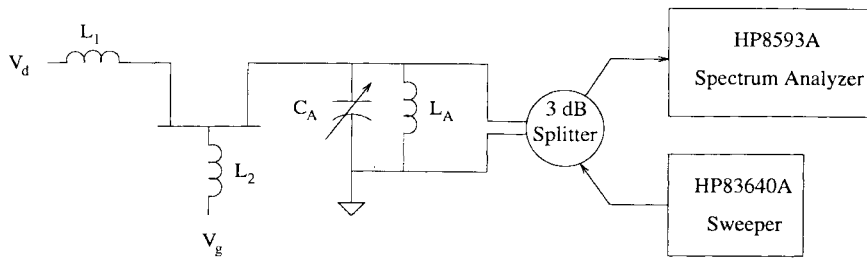


Fig. 2. Experimental setup used for testing the authors' model. Slight modification from the circuit in Fig. 1 allows the circuit to be tested using standard microwave equipment. The sweeper is used as the injection-locking source.

system is locked to a drive signal is to perform a Poincaré section [15] of the state variables with respect to that signal. If the points of the Poincaré section repeat with a period  $n$ , then the oscillator is locked as an  $n$ -cycle to the drive signal.

The number of state variables depends on the complexity of the model. Since, in modeling injection-locked oscillators, the important feature is how the output responds to the locking signal, the output voltage and its derivative are chosen as the state variables to be examined. In addition, the Poincaré section is taken every time the drive voltage crosses 0 V going from negative to positive. This usually occurs between two simulation points, so linear interpolation is used to estimate the precise location of the sectioned points.

Because the steady-state dynamics of the oscillator are what is of interest in this sweep, the simulation must continue long enough to allow the initial transient response to sufficiently decay before sectioning begins. The necessary delay strongly depends on the system being studied.

Once the transient response has decayed, the location of the sectioned point is compared with the three previous sectioned points using an averaged  $L_2$  norm [16]. The step for those previous sectioned points is equal to the number of the periodicity being checked, so that the error for an  $i$ -cycle test at the  $n$ th sectioning is

$$\text{error}_i^n = \frac{1}{3} \left[ (v_{\text{out}}^n - v_{\text{out}}^{n-i})^2 + (\dot{v}_{\text{out}}^n - \dot{v}_{\text{out}}^{n-i})^2 + (v_{\text{out}}^n - v_{\text{out}}^{n-2i})^2 + (\dot{v}_{\text{out}}^n - \dot{v}_{\text{out}}^{n-2i})^2 + (v_{\text{out}}^n - v_{\text{out}}^{n-3i})^2 + (\dot{v}_{\text{out}}^n - \dot{v}_{\text{out}}^{n-3i})^2 \right]^{1/2}$$

where  $v_{\text{out}}^n$  is the voltage across the tank circuit at the  $n$ th sectioning and the dots over the variables represent derivatives with respect to time.

This error is accumulated and then averaged to give the error per section for each periodicity. A discrimination level of 0.01 is chosen to signify a locked condition. This paper's investigation is limited to discriminating oscillations with periodicity of 1 through 7. The authors' feel that investigating higher period oscillations would do little to further understanding of system dynamics and enable improvements in design techniques, so that the added time and storage requirements that classifying larger periodicities would have entailed are not appropriate.

In addition, as discussed below in Section VI, it is difficult to truly establish the presence of chaotic signals. The large additional computational demands of automatically discerning

TABLE I  
COMPONENT VALUES FOR MEASURED CIRCUIT

$L_1$	=	60 nH
$L_2$	=	30 nH
$L_3$	=	15 nH
$C_{A,max}$	=	20 pF

modes which might be chaotic are not necessary for the purposes here.

### III. EXPERIMENTAL RESULTS

The oscillator circuit is a source-load oscillator circuit built around the NE71083 MESFET, surface-mounted inductors, and variable capacitors. This circuit is tested using the setup shown in Fig. 2. The component values used are shown in Table I.

The biasing is provided through lumped inductors to the gate and drain of the transistor, and the source is connected to ground by a lumped inductor and a variable capacitor (which provides some tuning ability). For the source load, a coaxial connection to a 3-dB power splitter allows both the sweeper and the spectrum analyzer to be connected to the circuit. The sweeper is the injection-locking source for the circuit, and the analyzer is used to examine the output waveforms. The circuit was biased at  $V_{DS} = 3$  V and  $I_{DS} = 35$  mA, which is roughly the bias condition at which the manufacturer's model data had been taken. The free-running oscillation was at 0.45 GHz with an amplitude of 0.1 mV.

The results of the experimental sweep of the injection-locking parameters are shown in Fig. 3. The primary features of this sweep are a main lobe, shown in black in the figure, where the oscillator locks with period one. This main lobe is significantly asymmetric. In addition, there is another lobe for higher drive frequencies and amplitudes, which demonstrates locking with a variety of different periods.

Output spectra for some injected signals show the type of subharmonics expected from multicycle oscillators; they also show the broad spectra that are often seen in chaotic systems, as can be seen in Figs. 4 and 5, respectively. The apparently chaotic spectra are seen in a variety of locations, especially where there are transitions from unlocked to locked states. The implications of the existence of multicycle and chaotic oscillations are discussed in the section below on time-domain results.

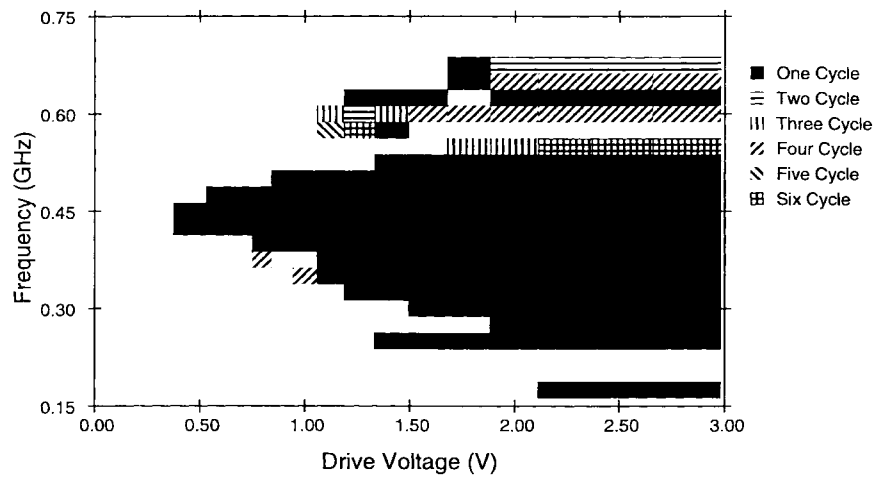


Fig. 3. Experimental sweep results. The free-running oscillation had an amplitude of 0.1 mV. The horizontal axis is the injection-locking signal amplitude.

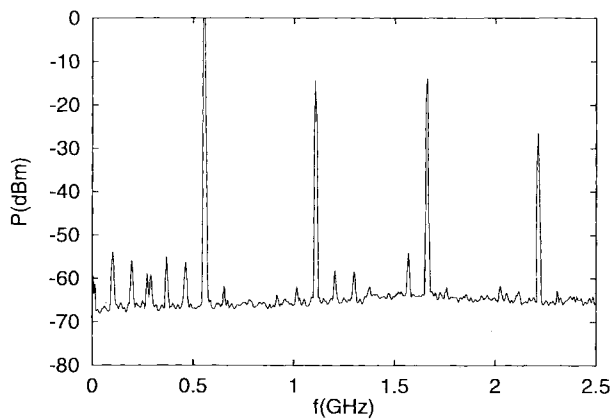


Fig. 4. Measured spectrum showing subharmonics indicative of multicycle (six-cycle) behavior. The injection signal is 0.9 V at 350 MHz.

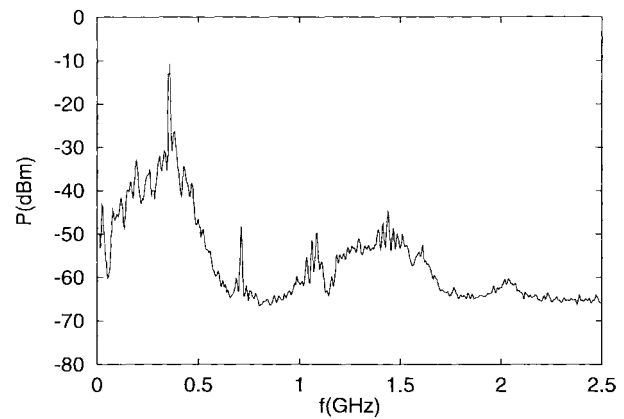


Fig. 5. Measured spectrum showing what is believed to be chaotic behavior. The injection signal is 2.2 V at 550 MHz.

#### IV. VAN DER POL OSCILLATOR MODEL

The van der Pol oscillator equation [17] is widely used to model nonlinear oscillator behavior. While this equation does not physically model the dynamics of MESFET oscillators, it is often used as a general model for the output voltage of these circuits.

For this paper, the authors used a generalized form of the equation, specifically

$$\frac{d^2v}{dt^2} = (\alpha - \beta v^2) \frac{dv}{dt} - \omega_0^2 v + A \cos(\omega_d t + \phi). \quad (1)$$

The equation parameters are chosen to be  $\alpha = 1.0$ ,  $\beta = 50$ , and  $\omega_0 = 3.45$ . The swept parameters are  $A$  and  $\omega_d$ . These choices make the free-running characteristics of the oscillator model comparable to those from both the circuit described above and the more complex model presented later. Equation (1) is implemented in Fortran and numerically solved using an adaptive fourth-order Runge-Kutta ordinary differential-equation solver [18].

The results of the sweep are shown in the parameter-space portrait in Fig. 6. There is a single, roughly symmetric lobe of one-cycle behavior and a few scattered areas of multicycle behavior. As these are all isolated points, it is believed that they represent spurious behavior that would be eliminated by

lengthening the simulation and allowing the error to increase to be above the cutoff point.

The main problem with these results is that the lobe of multicycle behavior seen in the experimental results does not appear in this model; moreover, the main lobe does not reflect the asymmetry of the experimental results.

It was expected that the van der Pol results would significantly differ from the experimental results, because the assumption that the MESFET can be treated as a negative resistance (as is roughly done for the van der Pol equation) is not accurate for MESFET oscillators in general. This equation adequately models some forms of common-source geometries, where the gate-drain capacitances are high enough to cause the gate-drain voltage to tend to be zero. The approximation is much less appropriate for other topologies, where the capacitances are much smaller between the two ports. In the source-load geometry, the reduction to a nonlinear negative resistance is too much of a simplification, as it does not take into account the nonlinear reactance.

#### V. SOURCE-LOAD OSCILLATOR MODEL

To model the circuit more realistically requires a more accurate nonlinear transistor model. Because of its wide-

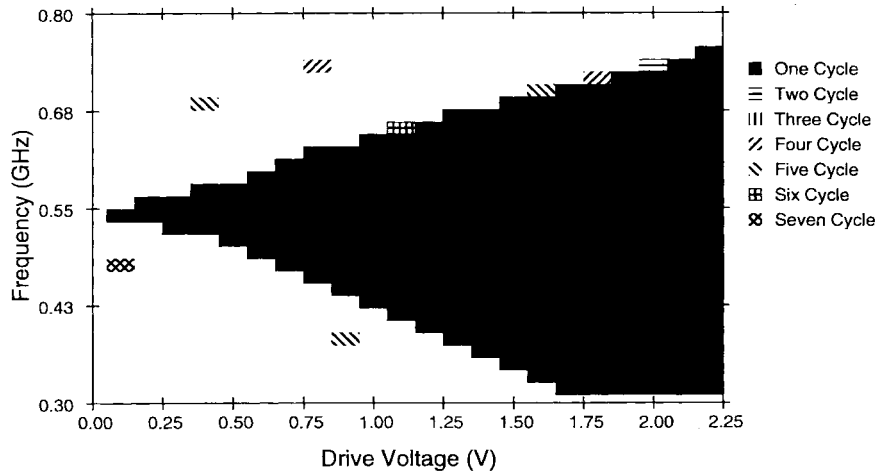


Fig. 6. Van der Pol locking sweep. The free-running peak-to-peak amplitude of the oscillation is 0.568 V.

spread use and the availability of model parameters, the Curtice–Cubic model [19] is employed for the drain–source current of the MESFET. The gate–source and gate–drain junctions are modeled by voltage-dependent capacitances in parallel with voltage-dependent resistances. This transistor model is inserted into the topology of Fig. 1, and nodal current analysis is used to derive a set of three coupled differential/integral equations, the solutions of which are the voltages at the three nodes in Fig. 1.

In order to avoid singularities in later mathematical manipulation, the voltage differences  $u_1$ ,  $u_2$ , and  $u_3$ , defined by

$$\begin{aligned} u_1 &= v_1 - v_2 \\ u_2 &= v_3 - v_2 \\ -u_3 &= v_s - v_2, \end{aligned}$$

are substituted into these coupled equations. Differentiating the nodal equations with respect to time and grouping like terms together yields the following system of second-order differential equations:

$$\begin{aligned} \ddot{u}_1(C_{gd} + C_{ds}) - \ddot{u}_2C_{gd} &= f \\ -\ddot{u}_1C_{ds} - \ddot{u}_2C_{gs} + \ddot{u}_3C_A &= g \\ -\ddot{u}_1C_{gd} + \ddot{u}_2(C_{gd} + C_{gs}) &= h \end{aligned} \quad (2)$$

where the dots above variables indicate derivatives with respect to time, and  $f$ ,  $g$ , and  $h$  are defined by

$$\begin{aligned} f &= -\dot{I}_{ds} - \frac{1}{L_1}(u_1 + u_3 + v_s - v_d) \\ &\quad - (\dot{C}_{gd} + G_{gd})(\dot{u}_1 - \dot{u}_2) - \dot{G}_{gd}(u_1 - u_2) \\ g &= \dot{I}_{ds} + (\dot{C}_{gs} + G_{gs})\dot{u}_2 + \dot{G}_{gs}u_2 - \frac{\dot{u}_3 - \dot{v}_A}{R_A} - \frac{u_3}{L_A} \\ h &= -\frac{1}{L_2}(u_2 + u_3 + v_s) - (\dot{C}_{gd} + G_{gd})(\dot{u}_2 - \dot{u}_1) \\ &\quad - \dot{G}_{gd}(u_2 - u_1) - (\dot{C}_{gs} + G_{gs})\dot{u}_2 - \dot{G}_{gd}u_2. \end{aligned}$$

Using standard linear algebraic techniques on the coefficients of the left-hand side (LHS) in order to separate the

second-order differential terms from each other results in the following set of equations:

$$\begin{aligned} \ddot{u}_1 &= \frac{k_1(f + C_{gd}h')}{k_2} \\ \ddot{u}_2 &= \frac{C_{gd}}{k_2}(f + C_{gd}h') + h' \\ \ddot{u}_3 &= \frac{1}{C_A}(f + g + h) \end{aligned} \quad (3)$$

where

$$\begin{aligned} k_1 &= C_{gd} + C_{gs} \\ k_2 &= C_{gs}C_{gd} + C_{ds}C_{gd} + C_{gs}C_{ds} \\ h' &= \frac{h}{k_1}. \end{aligned}$$

Equation (3) is implemented in Fortran using the same adaptive Runge–Kutta solver and parameter sweep program mentioned above.

For the simulations, parameter values were chosen to match the NE71083 MESFET, as shown in Table II. The tank circuit parameters are  $R_A = 50 \Omega$ ,  $C_A = 30$  pF, and  $L_A = 15$  nH, and the external inductors are  $L_1 = 60$  nH and  $L_2 = 25$  nH. The biases are  $V_{ds} = 2.9$  V and  $V_{gs} = -0.1$  V, which gives conditions very close to those where the Curtice–Cubic model was made. With these choices, the free-running oscillation is about 500 MHz, which is within 16% of the free-running frequency of the physical circuit.

This circuit is simulated at 682 different combinations of injection frequency and magnitude, with a precision level of  $10^{-7}$ , to an end time of 160 ns. The sectioning starts after 40 ns to allow the initial transients to settle. The entire sweep takes approximately 170 h of computing time on HP-700 series workstations.

The results from the simulation are shown in Fig. 7. Whereas the behavior of the van der Pol model was too simple, the Curtice–Cubic behavior appears to be somewhat too complex. The main lobe shows the same asymmetry seen in the experiment, and the plot also shows the type of higher period orbits which appear in the experiment. Two other lobes also appear. These, together with the main lobe, correspond

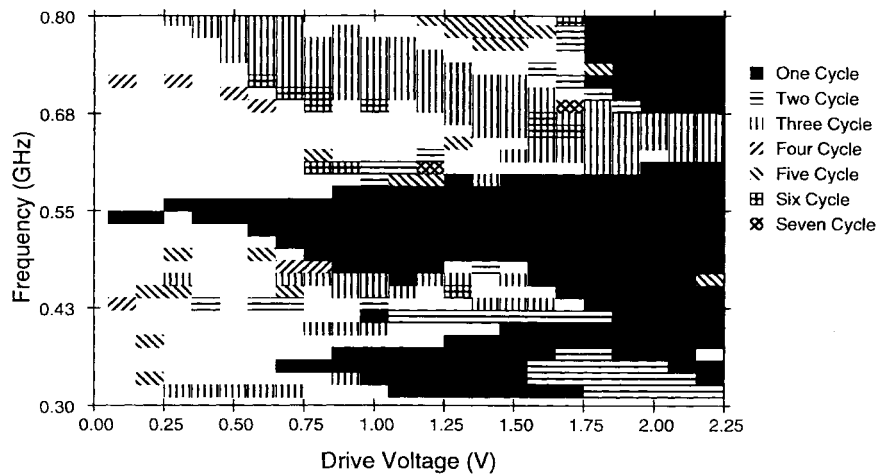


Fig. 7. Curtice model injection locking sweep. The free-running peak-to-peak amplitude of the oscillation is 0.449 V.

TABLE II  
CURTICE-CUBIC MODEL PARAMETERS FOR THE NE710 SERIES, AS  
PROVIDED BY THE MANUFACTURER. THE MODEL PARAMETERS ARE  
BASED ON MEASUREMENTS AT  $V_{ds} = 3$  V AND  $I_{ds} = 30$  MA

$C_{gs0}$	$= 0.45$ pF
$C_{gd0}$	$= 0.1$ pF
$v_{bi}$	$= 0.6516$ V
$\gamma$	$= 1.63$ V <sup>-1</sup>
$A_0$	$= 0.0563$ V <sup>-1</sup>
$A_1$	$= 0.1022$ V <sup>-1</sup>
$A_2$	$= 0.0619$ V <sup>-1</sup>
$A_3$	$= 0.00383$ V <sup>-1</sup>
$\beta$	$= 0.047$ V <sup>-1</sup>
$v_{ds0}$	$= 2.72$ V
$C_{ds}$	$= 0.135$ pF
$I_s$	$= 7.31 \times 10^{-12}$ A
$nv_t$	$= 0.03146$ V

to three separate areas where the injection amplitude and frequency combine to cause locking behavior. In addition, there are a number of other isolated areas that show some degree of locking.

The primary lobe is fairly narrow and consists of one-cycle oscillations. This is the most commonly used injection-locking regime, because the oscillator will lock completely to the injected signal. The upper secondary lobe shows locking as a three-cycle oscillator, with bifurcations at higher injection amplitudes to six-cycle oscillations (e.g., near 0.68 GHz and 0.75 or 1.75 V). Further bifurcations to 12-cycle oscillations probably exist, but the authors' program does not identify these. This upper lobe, at low drive levels, starts at a frequency of about 3/2 the free-running frequency and decreases in frequency as the drive voltage is increased. The lower secondary lobe initially looks quite similar to the main lobe, but bifurcates to two-cycle oscillation as the drive voltage increases. This lobe is at roughly 2/3 of the free-running frequency; unlike the upper lobe, it does not show a frequency

shift with increased drive voltage. In the region where the drive voltage is between 1.0 and 1.75 V and the drive frequency is between 0.40 and 0.48 GHz, the behavior is seen to be quite erratic, with many different locking modes present. This is typical of regions where chaotic behavior might be present. Based on the experimental results, chaotic behavior is expected to be present along the locking boundaries, but experiments were not performed to confirm or deny this expectation.

## VI. TIME-DOMAIN RESULTS

As described in the previous section, the Curtice-Cubic model describes much of the actual steady-state dynamics of the locked system. The next stage of the model verification process is to examine results in the time domain for a selection of injected signals that show interesting and representative behavior.

At the first such parameter-space setting (0.54 GHz, 1.0 V), the signal converges to a period-one limit cycle, as shown in Figs. 8–10. When the frequency is raised to 0.73 GHz, this one-cycle bifurcates to a three-cycle. Figs. 11–13 show these results. The frequency spectrum in Fig. 13 is similar to that shown experimentally in Fig. 4 with respect to the prominent subharmonics, although with a different periodicity. The thickness of the lines in Fig. 12 indicates that the system has not completely settled, and could be eliminated if the simulation time was increased significantly.

If, on the other hand, the frequency is lowered to 0.46 GHz and the amplitude is raised to 1.4 V, the behavior is apparently chaotic, as seen in Figs. 14–16. The results in Figs. 14–16 can only tentatively be classified as chaos because there is no reasonable way to *prove* the existence of chaos in a system of this complexity. That chaos should be present is expected as an extension of [20], but that paper only strictly applies to one-dimensional (1-D) discrete mappings. For more complicated systems, methods like those of Melnikov [21], [22] can sometimes be used, but these are based on formally establishing the presence of horseshoes (stretching and folding) in the phase-space flow, a difficult task in high-dimensional systems, and an all-but-impossible one in experimental systems.

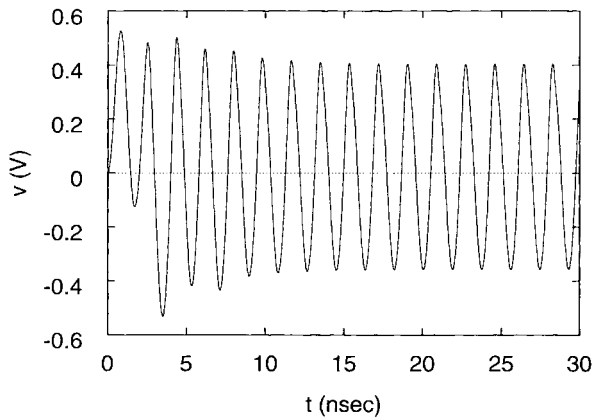


Fig. 8. One-cycle oscillation time domain. The oscillator is injected with a 0.54 GHz 1.0 V signal.

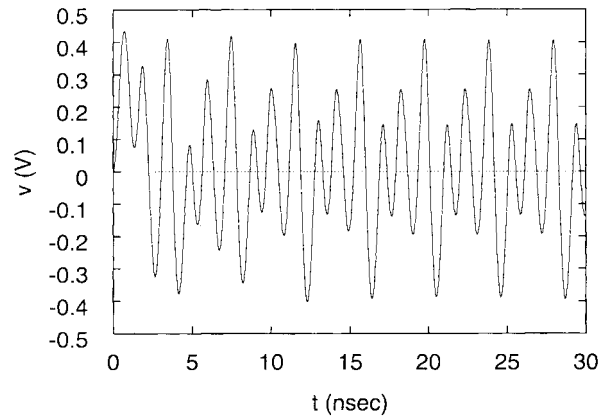


Fig. 11. Three-cycle oscillation time domain. The injection signal is at 0.73 GHz and 1.0 V.

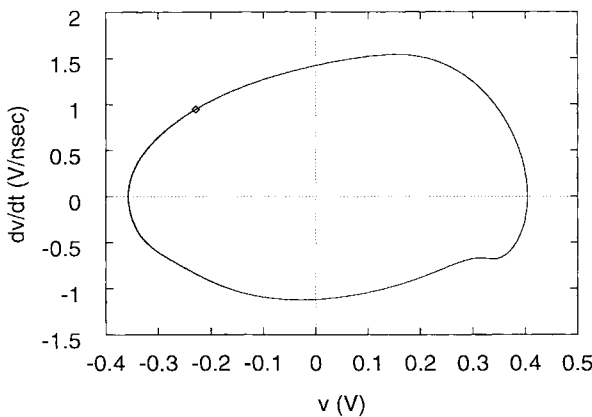


Fig. 9. One-cycle oscillation phase space. This has the same injection signal as in Fig. 8. The markers indicate the points of the Poincaré sectioning.

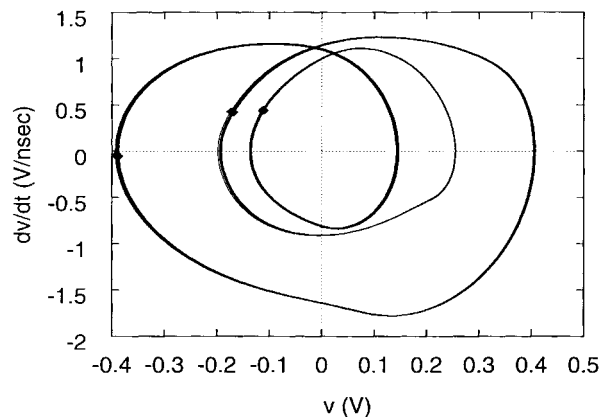


Fig. 12. Three-cycle oscillation phase space. The injection signal is as in Fig. 11. The markers indicate the points of the Poincaré sectioning. The thickness of the lines indicates that the system has not completely settled, which could be eliminated with significantly longer execution times.

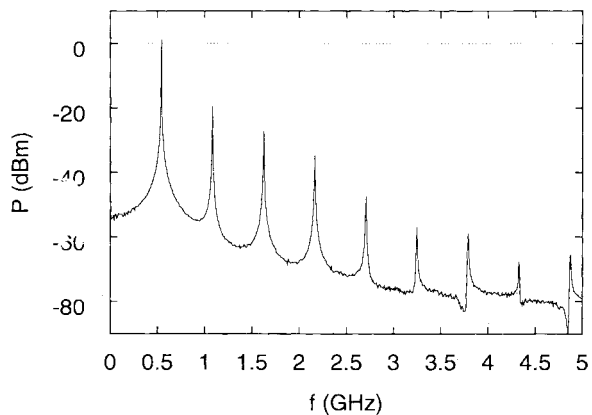


Fig. 10. One-cycle oscillation frequency domain. This again uses the same parameters as in Fig. 8. The noise floor is due to discretization noise in the fast Fourier transform (FFT).

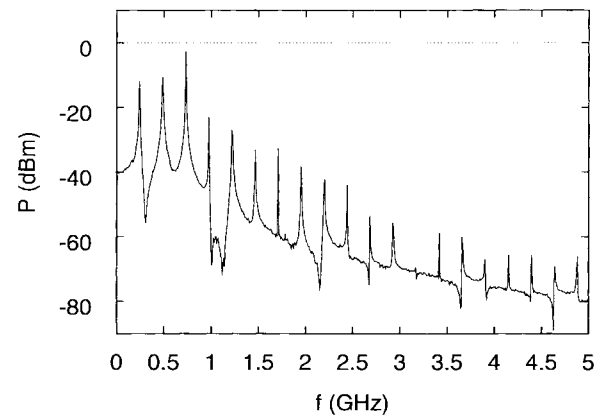


Fig. 13. Three-cycle oscillation frequency domain. The parameters are again as in Fig. 11. The noise floor is roughly the same as Fig. 10. The power in the fundamental frequency is much less than seen in Fig. 10.

As is apparent in Fig. 15, the phase-space attractor exhibits some fractal structure.<sup>1</sup> Fig. 16, viewed in comparison to Figs. 10 and 13, shows the classic broad noise-like spectrum that is also common in—and symptomatic of—chaotic systems [23], and which is similar to the experimental results in Fig. 5.

<sup>1</sup>That is, it resembles a Cantor set in cross section.

The results shown here have several important implications, both for techniques to be used in detecting these effects in laboratory measurements and for the validity of assumptions made in other modeling methods. The presence of the subharmonics of multicycles and the frequency spreading for the apparently chaotic oscillations in Figs. 13 and 16 provides a straightforward

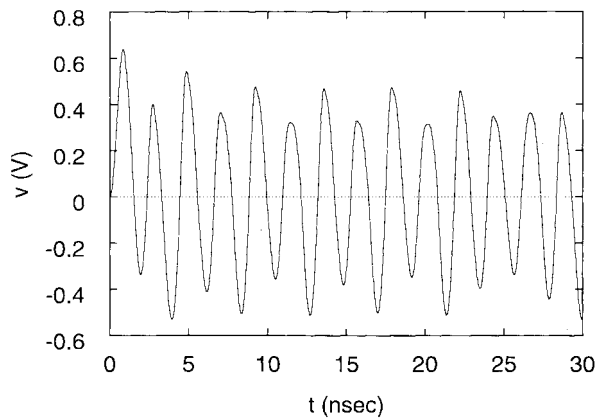


Fig. 14. Apparent chaotic oscillation time domain. The injected signal is 1.4 V at 0.46 GHz.

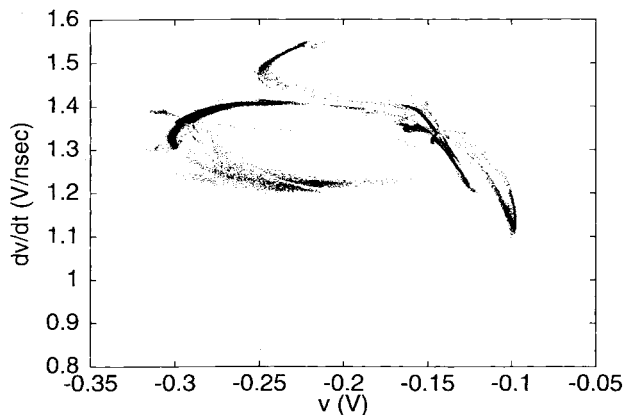


Fig. 15. Apparent chaotic oscillation, Poincaré section. The injected signal is the same as for Fig. 14. The fractal (Cantor set) characteristics of the section strongly suggests the system is chaotic.

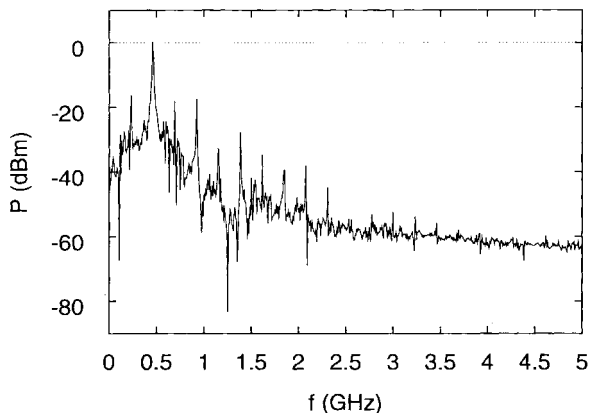


Fig. 16. Apparent chaotic oscillation frequency domain. The injected signal is as in Fig. 14. The spectrum is spread much rougher, and has a higher background level than Figs. 10 and 13. This is a feature common in chaotic systems.

ward method for detecting these behaviors using a spectrum analyzer. Direct detection of these types of oscillations in the time domain is difficult at microwave frequencies.

The frequency-domain plots show that the power at the locking frequency is significantly decreased when the circuit is operating in multicycle and apparently chaotic regimes,

since more power is lost to frequencies other than the locking frequency. This means that single-cycle oscillators should be used when the object is to maximize the power at the injected frequency. It is not presently clear whether the presence of these subharmonics can be exploited in some useful manner.

The significant subharmonics seen in Figs. 4 and 13 and the broad spectra of Figs. 5 and 16, challenge the assumption that the amplitude of the signal is varying slowly with respect to the carrier frequency. This calls into question whether forms of nonlinear analysis which use this assumption, as in [4], can accurately model the dynamics of transistor oscillators. These frequency characteristics also cause problems for techniques that employ a finite sum of frequency components, such as harmonic balance and Volterra series analysis. The subharmonics from the oscillators would require the use of subharmonics in these analyses, but there is no way to know *a priori* what periodicity to expect. The broad spectrum of the chaotic signal would require an infinite number of frequencies to be properly simulated, so any of these methods would fail.

## VII. CONCLUSION

A time-domain analysis of injection-locked microwave transistor oscillators using a nonlinear device model is presented. The results are compared to an analysis using a simpler van der Pol oscillator model and to an experimental model. It is concluded that the van der Pol model does not accurately characterize a general microwave transistor oscillator, since it does not take into account the nonlinear reactive part of the device impedance, but treats the transistor as a nonlinear negative resistance. However, it is possible to choose the circuit elements and oscillator topology such that the van der Pol model will model certain oscillator behaviors. The analysis using a Curtice–Cubic transistor model qualitatively predicts the behavior of a 0.5-GHz experimental model.

Injection-locked oscillators are analyzed by using the Poincaré section in an automated numerical procedure. It is shown that commonly used nonlinear dynamics techniques, such as the phase-space portrait, can provide a useful tool for understanding microwave oscillators.

The van der Pol and Curtice–Cubic models give significantly different results when the injection-locked frequency is plotted against injection-locking signal power. The van der Pol model yields a symmetrical plot around the free-running frequency, which is shown not to be the case in realistic experimental oscillators. The asymmetries in the injection-locking plane are better predicted using a nonlinear transistor model.

Both numerical and experimental results are presented, showing multicycle behavior, as well as what is believed to be chaotic behavior, in a very simple microwave oscillator. These behaviors can be identified by the subharmonics or spectral broadness seen in spectrum plots. The existence of such behavior can cause problems for traditional nonlinear analysis techniques, which assume a finite number of harmonics or slowly varying time-domain amplitudes and phases. This can dramatically affect the circuit performance.

The approach presented is intended to help the understanding of nonlinear circuit behavior rather than to serve as a design tool. However, the authors feel that nonlinear time-domain analysis can be useful for designing microwave oscillators, since it can predict regions of potential multicycle (or chaotic) oscillations for a given oscillator topology. It can also give insight as to how the embedding circuit can be changed to avoid this type of behavior within a given injection-locking frequency range. Since this is a time-domain representation of the circuit, it could be integrated with finite-difference time-domain codes for a more complete electromagnetic analysis of high-frequency (HF) oscillators.

#### ACKNOWLEDGMENT

The authors would like to thank NEC California Eastern Laboratories for their transistor donation, KOA Speer Electronics for their inductor donation, and Voltronics for their capacitor donations.

#### REFERENCES

- [1] D. B. Rutledge, Z. B. Popović, R. M. Weikle, II, M. Kim, K. A. Potter, R. York, and R. C. Compton, "Quasi-optical power combining arrays," in *IEEE MTT-S Int. Microwave Symp. Dig.*, Dallas, TX, May 1990, pp. 1201–1204.
- [2] W. A. Shiroma, B. L. Shaw, and Z. B. Popović, "A 100-transistor quadruple grid oscillator," *IEEE Microwave Guided Wave Lett.*, vol. 4, pp. 350–351, Oct. 1994.
- [3] W. A. Shiroma, S. C. Bundy, S. Hollung, B. D. Bauernfeind, and Z. B. Popović, "Cascaded active and passive quasi-optical grids," *IEEE Trans. Microwave Theory Tech.*, vol. 43, pp. 2904–2909, Dec. 1995.
- [4] R. A. York, "Nonlinear analysis of phase relationships in quasi-optical oscillator arrays," *IEEE Trans. Microwave Theory Tech.*, vol. 41, pp. 1799–1809, Oct. 1993.
- [5] A. Balasubramanian, J. Heinbockel, A. Mortazawi, and T. Itoh, "A periodic spatial power combining MESFET oscillator," *IEEE Trans. Microwave Theory Tech.*, vol. 43, pp. 1196–1197, May 1995.
- [6] P. Liao and R. A. York, "A 1-W X-band power combining array using coupled VCO's," in *IEEE MTT-S Int. Microwave Symp. Dig.*, San Diego, CA, May 1994, pp. 1235–1238.
- [7] R. D. Martinez and R. C. Compton, "High-efficiency FET/microstrip-patch oscillators," *IEEE Trans. Antennas Propagat.*, vol. 36, pp. 16–19, Feb. 1994.
- [8] B. K. Kormanyos and G. M. Rebeiz, "20-GHz power combining slot-oscillator array," in *IEEE AP-S Symp. Dig.*, Seattle, WA, 1994, pp. 840–843.
- [9] P. Liao and R. A. York, "A six-element beam-scanning array," *IEEE Microwave Guided Wave Lett.*, vol. 4, pp. 20–22, Jan. 1994.
- [10] P. S. Hall and P. M. Haskings, "Microstrip active patch array with beam scanning," *Electron. Lett.*, vol. 28, no. 22, pp. 2056–2057, Oct. 1992.
- [11] G. D. Vendelin, A. M. Pavio, and U. L. Rohde, *Microwave Circuit Design*. New York: Wiley, 1990, pp. 653–667.
- [12] C.-C. Huang and T.-H. Chu, "Analysis of MESFET injection-locked oscillators in fundamental mode of operation," *IEEE Trans. Microwave Theory Tech.*, vol. 42, pp. 1851–1857, 1994.
- [13] R. A. York, P. Liao, and J. J. Lynch, "Oscillator array dynamics with broad-band  $N$ -port coupling networks," *IEEE Trans. Microwave Theory Tech.*, vol. 42, pp. 2040–2045, Nov. 1994.
- [14] D. D'Humieres, M. R. Beasley, B. A. Huberman, and A. Libchaber, "Chaotic states and routes to chaos in the forced pendulum," *Phys. Rev. A, Gen. Phys.*, vol. 26, pp. 3483–3496, Dec. 1982.
- [15] T. S. Parker and L. O. Chua, *Practical Numerical Algorithms for Chaotic Systems*. New York: Springer-Verlag, 1989, pp. 31–56.
- [16] G. Dahlquist and A. Björck, *Numerical Methods*. Englewood Cliffs, NJ: Prentice-Hall, 1974, pp. 85–87.
- [17] B. van der Pol, "The nonlinear theory of electric oscillators," *Proc. IRE*, vol. 22, pp. 1051–1085, Sept. 1934.

- [18] W. H. Press, S. A. Teukolsky, W. T. Vetterling, and B. P. Flannery, *Numerical Recipes in FORTRAN*, 2nd ed. Cambridge, U.K.: Cambridge Univ. Press, 1992, ch. 16, pp. 701–744.
- [19] W. R. Curtice and M. Ettenberg, "A nonlinear GaAs FET model for use in the design of output circuits for power amplifiers," *IEEE Trans. Microwave Theory Tech.*, vol. 33, pp. 1383–1394, Aug. 1985.
- [20] T.-Y. Li and J. A. Yorke, "Period three implies chaos," *Amer. Math. Monthly*, pp. 985–992, 1982.
- [21] P. Holmes, "Nonlinear oscillations and the smale horseshoe map," in *Chaos and Fractals: The Mathematics Behind the Computer Graphics* (Amer. Math. Soc.), in *Proc. Symp. Applied Math.*, Providence, RI, 1989, vol. 39, pp. 25–39.
- [22] J. Guckenheimer and P. Holmes, *Nonlinear Oscillations, Dynamical Systems, and Bifurcations of Vector Fields*. New York: Springer-Verlag, 1983.
- [23] B. A. Huberman and A. B. Zisook, "Power spectrum of strange attractors," *Phys. Rev. Lett.*, vol. 46, pp. 626–628, 1981.



**Jonathan Dixon** (S'89) received the B.S. degree in both electrical engineering and mathematics from Michigan State University, East Lansing, in 1992, and the M.S. and Ph.D. degrees in electrical engineering from the University of Colorado, Boulder, in 1993 and 1997, respectively.

Dr. Dixon is a member of Eta Kappa Nu and Tau Beta Pi and has received a Michigan State University Alumni Distinguished Scholarship, an Office of Naval Research Graduate Fellowship, and was an Honorable Mention for the Alton B. Zerber Outstanding Electrical Engineering Student Award in 1992.



**Elizabeth Bradley** (S'86–M'92) received the S.B., S.M., and Ph.D. degrees from the Massachusetts Institute of Technology, Cambridge, MA, in 1983, 1986, and 1992, respectively.

She joined the Department of Computer Science at the University of Colorado, Boulder, in 1993, as an Assistant Professor, with a joint appointment in electrical and computer engineering, and is also affiliated with the program in applied mathematics and the Department of Mechanical Engineering's Combustion Center. Her research interests are nonlinear dynamics and chaos, scientific computation and AI, network theory and circuit design, and classical mechanics.

Dr. Bradley is a member of Eta Kappa Nu, Tau Beta Pi, and Sigma Xi, and the recipient of a National Young Investigator Award and a Packard Fellowship.



**Zoya B. Popović** (S'86–M'90) received the Dipl. Ing. degree from the University of Belgrade, Serbia, Yugoslavia, in 1985, and the M.S. and Ph.D. degrees from the California Institute of Technology, Pasadena, in 1986 and 1990, respectively.

She is currently an Associate Professor in electrical and computer engineering at the University of Colorado, Boulder. Her research interests include microwave and millimeter-wave quasi-optical techniques, microwave and millimeter-wave active antennas and circuits, and electromagnetic modeling of antennas and circuits.

Dr. Popović is a recipient of the URSI Young Investigator Award and the NSF Presidential Faculty Fellow Award in 1993, and the URSI International Issac Koga Gold Medal in 1996. She is a winner of the 1993 IEEE Microwave Theory and Techniques Microwave Prize for pioneering work in quasi-optical grid oscillators.